

Record-breaking 2020 summer marine heatwaves in the western North Pacific



Yulong Yao^{a,b,c}, Chunzai Wang^{a,b,c,*}, Chao Wang^d

^a State Key Laboratory of Tropical Oceanography, South China Sea Institute of Oceanology, Chinese Academy of Sciences, Guangzhou, China

^b Global Ocean and Climate Research Center, Guangzhou, China

^c Innovation Academy of South China Sea Ecology and Environmental Engineering, Chinese Academy of Sciences, Guangzhou, China

^d Key Laboratory of Meteorological Disaster of Ministry of Education, Joint International Research Laboratory of Climate and Environment Change and Collaborative

Innovation Center on Forecast and Evaluation of Meteorological Disasters, Nanjing University of Information Science and Technology, Nanjing, China

ARTICLE INFO

Handling Editor: Dr. K Drinkwater

Keywords:

Marine heatwave
Western North Pacific
Inter-ocean interaction
Coral bleaching

ABSTRACT

Record-breaking marine heatwaves (MHWs) occurred in the western North Pacific during the summer of 2020. These unprecedented MHWs were consistent with favorable large-scale conditions that are linked to an anomalous western North Pacific subtropical high (WNPSH), resulting mainly from sea surface temperature (SST) anomalies across the tropical oceans. In addition, a moderate La Niña-like pattern was also conducive to transporting warm seawater to the western North Pacific. Mixed-layer heat budgets suggest that surface heat flux contributed to the SST anomaly in the western subtropical Pacific. In contrast, oceanic heat advection dominated in the South China Sea and the western equatorial Pacific. Numerical model experiments indicated that the tropical Indian Ocean SST anomalies were responsible for the enhanced WNPSH. The increased zonal SST gradient across the tropical Pacific also played an important role. Inter-ocean interactions can modulate climate variability through ocean-atmospheric coupling and deserve more attention when predicting MHWs within the context of global warming. In addition, it is critical to consider MHWs as a powerful tool in detecting acute, intense thermal stress events in the coral bleaching pre-warning system.

1. Introduction

Oceans absorb over 90% of the excessive heat that results from the greenhouse effect, and in 2020, both ocean heat content and the upper ocean temperature reached record levels (Cheng et al., 2017, 2019, 2021). Marine heatwaves (MHWs), discrete periods of anomalous warm seawater that exceed seasonality variation (Hobday et al., 2016), have a substantial impact on marine ecosystems (Holbrook et al., 2020b; Oliver et al., 2020; Smale et al., 2019). In recent decades, MHWs have occurred frequently in the western North Pacific (Gao et al., 2020; Yao et al., 2020), especially in strong El Niño years (Liu et al., 2022; Yao and Wang, 2021). Summer MHWs pose serious ecological risks to South Asia's coral reefs, which account for 30% of the world's coral reefs (Souter et al., 2022). For example, massive coral bleaching events occurred in the South China Sea during the summer of 2020 (Chen et al., 2022; Feng et al., 2022; Licuanan and Mordeno, 2021; Lyu et al., 2022; Mo et al., 2022; Szeredy and Amri, 2021).

The El Niño-Southern Oscillation (ENSO) plays a substantial role in

influencing the likelihood of MHWs through an atmospheric and oceanic pathway in the Indo-Pacific region (Holbrook et al., 2019, 2020a; Oliver et al., 2018). During El Niño's decaying summer, an anomalous anti-cyclonic circulation forms over the western North Pacific, a prime system affecting the East Asian monsoon (Li et al., 2017; Wu et al., 2017). Warm sea surface temperature anomalies and severe MHW events over the western North Pacific are linked to this high-pressure system and its corresponding anticyclonic circulation (Chen et al., 2022; Feng et al., 2022; Mo et al., 2022; Tan and Cai, 2018; Yao and Wang, 2021). An anomalous anticyclone reduces cloud cover, enhances insolation, suppresses wind speeds, and results in hot, dry weather (Holbrook et al., 2020b). However, El Niño was in a weak phase during the winter of 2019/20, with the running 3-month mean ENSO 3.4 index in December-January-February of only 0.5 °C, compared to 2.2 °C and 2.5 °C in the winters of 1997/98 and 2015/16, respectively. The Pacific SSTs evolved from a weak El Niño condition in the previous winter into a moderate La Niña in September 2020 (Fig. S1a).

The weak intensity of the 2019/20 El Niño event suggests that it had

* Corresponding author. 164 West Xingang Road, Guangzhou, 510301, China.

E-mail address: cwang@scsio.ac.cn (C. Wang).

a minimal effect on MHW occurrences in the western North Pacific during the summer of 2020. According to previous studies, the Indian Ocean warming caused an abnormal anticyclonic circulation in the western North Pacific during the summer of 2020 (Fig. S1b). This resulted in historic Yangtze River flooding between June and July and a record absence of tropical cyclones in the western North Pacific in July (Wang et al., 2021; Zhou et al., 2021). However, even though the mechanisms responsible for the anomalous western North Pacific subtropical high (WNPSH) have been extensively discussed, its impact on the extreme MHWs in the western North Pacific during the summer of 2020 has not been fully explained.

This study investigated the physical causes of the record-breaking summer MHWs (June-July-August) in the western North Pacific. The event was described in terms of sea surface temperature (SST) anomalies and total MHW days in summer of 2020. The role of anomalous WNPSH and global tropical SST patterns is investigated via a mixed-layer heat budget analysis and numerical experiments. The results provide a more comprehensive understanding of inter-ocean interactions affecting MHWs and their potential ecological impacts on coral reefs.

2. Data and methods

2.1. Observational and reanalysis data

The daily SSTs are from the Optimum Interpolation SST version 2.1 data set (OISST v2.1), which provides a $0.25^\circ \times 0.25^\circ$ global grid from September 1981 to the present. This data set is an interpolation of remotely sensed SSTs from the Advanced Very High-Resolution Radiometer imager, as provided by the National Oceanic and Atmospheric Administration (NOAA) (Huang et al., 2021). Monthly SSTs from NOAA Extended Reconstruction SST version 5 (ERSST5) are also analyzed (Huang et al., 2017). The NOAA OISST product series was found to be the best among the other SST products in comparison with in situ SST observations (Liu et al., 2018). The degree heating weeks index combines the magnitude and duration of SST exceeding the maximum of the monthly means, which is monitored by NOAA Coral Reef Watch (Liu et al., 2014). Degree heating weeks (DHWs) of 4°C -weeks and 8°C -weeks indicate bleaching-level thermal stress and mortality-level thermal stress, respectively. Here we use a daily 5-km degree heating weeks product in summer of 2020 to evaluate the status of coral reefs in the western North Pacific.

The ERA5 is the fifth-generation of the European Centre for Medium-Range Weather Forecasts (ECMWF) atmospheric reanalysis of the global climate, which provides hourly estimates of many atmospheric, land, and oceanic variables from 1979 to the present. The variables of monthly SST, 10-m wind speed, total precipitation, surface net solar radiation, surface latent heat flux, top net thermal radiation, and 500-hPa and 850-hPa geopotential heights with corresponding horizontal winds are used to construct an overview of large-scale conditions in summer 2020.

NCEP Global Ocean Data Assimilation System (GODAS) is a real-time monthly ocean analysis and reanalysis with 40 vertical levels in the model with $1^\circ \times 1/3^\circ$ resolution. The variables of potential temperature, geometric vertical velocity, u- and v-component currents, salinity, and total downward heat flux at the surface are used to calculate the mixed layer heat budget (Huang et al., 2010). NCEP-DOE reanalysis 2 is an improved version of the NCEP Reanalysis 1 model that corrects many known problems (Kanamitsu et al., 2002). NCEP-DOE reanalysis 2 offers triangular spectral resolution on the T62 grid from January 1979 to the present. Monthly mean solar radiation flux, longwave radiation flux, latent heat flux, and sensible heat flux are used to analyze the contribution of each heat flux to the development of MHWs in summer of 2020.

2.2. Methods

2.2.1. Definition of marine heatwaves

According to Hobday et al. (2016), MHWs are defined as discrete, prolonged, and anomalously warm seawater events that exceed the daily 90th percentile for at least five consecutive days. We calculate the climatological threshold based on data collected for 01/01/1982–12/31/2020, using an 11-day window centered on that day, and then smoothed with a 31-day moving average. Although this seasonally varying threshold can identify MHWs at any time of the year, only those occurring during summer (June-July-August) are considered. We used four indices to represent the characteristics of the MHWs, including total MHW days (HWT), average MHW duration (HWDU), the number of MHWs (HWN), and average MHW intensity (HWI) (Table 1).

2.2.2. Ocean mixed-layer heat budget calculation

We calculate a monthly mixed layer heat budget from GODAS to diagnose the dynamic and thermodynamic processes controlling temperature variability during MHWs. The heat budget equation can be written as follow:

$$\frac{\partial T'}{\partial t} = -(\mathbf{V} \cdot \nabla T)' + \frac{Q'_{\text{net}}}{\rho_0 C_p H} + \text{Residual}$$

where $(\cdot)'$ indicates monthly mean anomalies, T denotes the mixed layer temperature, \mathbf{V} the three-dimensional ocean current, and ∇ the gradient operator. Q_{net} is the net surface heat flux into the ocean, and ρ_0 and C_p are the water density and specific heat capacity, respectively (Zhu and Kumar, 2018). The advection term $-(\mathbf{V} \cdot \nabla T)'$ in equation can be further decomposed into six parts, the details can be found in Fan et al. (2019). Moreover, the mixed layer depth (H) is calculated as a constant at 50 m (Zhu and Kumar, 2018; Fan et al., 2019) because the heat budget results are insensitive to the mixed layer depth, and the residual term is more minor. The baseline period is from 1982 to 2020.

2.2.3. Atmospheric global climate model

As part of the IPCC Fourth Assessment Report, the Max Planck Institute for Meteorology developed the fifth-generation atmospheric general circulation model (ECHAM5). The model is run at a horizontal resolution of 42 spectral triangular and 31 vertical levels in a hybrid sigma-pressure coordinate system (Roeckner et al., 2003). In this study, the ECHAM 5.3 model is used to investigate the impacts of trans-basin SST anomalies, across the tropical oceans, on large-scale circulation in the western North Pacific (Wang et al., 2021). The control run was driven by climatological monthly average SST and sea ice data from

Table 1
Definitions of MHW indices.

Index	Definition	Formulas	Unit
HWN	Summer total number of MHW events within a year	$\text{HWN} = N$	Counts
HWT	Summer total MHW days within a year	$\text{HWT} = \sum_{i=1}^N D_i$	Days
HWDU	Average duration of MHW events in summer within a year	$\text{HWDU} = \sum_{i=1}^N (D_i) / N$	Days/count
HWI	Average intensity of MHW events in summer within a year	$\text{HWI} = \sum_i^N \sum_j^{D_i} (T_{ij} - \bar{T}_{ij}) / N$	°C day/count

Note: for an MHW i , its intensity $\sum_j^{D_i} (T_{ij} - \bar{T}_{ij})$ is calculated as the sum of the temperature deviation exceeding the threshold throughout its duration D_i . T_{ij} and \bar{T}_{ij} are the SST and corresponding threshold for day j during MHW i (Yao and Wang, 2021).

1980 to 2010. The sensitivity run was the same as the control run except that the tropical SST anomalies (20°S–30°N) from June to August 2020 were added to the corresponding climatological monthly SST. The SST warming associated with anomalous WNPSH results from atmospheric forcing, so only SST anomalies outside the scope of anomalous WNPSH were included in the sensitivity experiment. Both the control and sensitivity experiments were integrated for 32 years. Because the SST anomalies remain unchanged in time in the sensitivity experiment, the experiments are equivalent to 32-member ensemble runs. The outputs of the last 30 years were used to construct the 30 ensemble members (Wang et al., 2021).

3. Results

3.1. Extreme marine heatwaves in the western North Pacific

In summer of 2020, HWT was high in the South China Sea (blue box),

110°E–120°E, 5°N–15°N), western subtropical Pacific (green box, 135°E–148°E, 20°N–27°N), and western equatorial Pacific (black box, 140°E–150°E, 2°S–7°N), ranging from 60 to 92 days (Fig. 1a). Having examined the historical summer average SST anomalies in three boxes since 1982, summer of 2020 has the highest values (around 1.0 °C); after considering detrended SST anomalies over the past 39 years, summer of 2020 is still one of the highest years (Fig. 1b–d). The unprecedented high SST anomaly in summer of 2020 resulted in the HWT exceeding five standard deviations in all boxes from 1982 to 2020 (Fig. 1e–g). Meanwhile, the summer average SST anomaly over the western North Pacific in 2020 was also significantly positive, reaching 1.0–1.8 °C in three boxes (Fig. 2a). Like the HWT spatial distribution pattern, the values of HWUD and HWN are also high in the South China Sea, western subtropical Pacific, and western equatorial Pacific, ranging from 30 to 60 days/count to 3–6 counts, respectively (Fig. 2b–c). High HWI is concentrated in the northern part of the western North Pacific and exceeds 1.5 °C day/count, increasing from the low-latitude to the high-

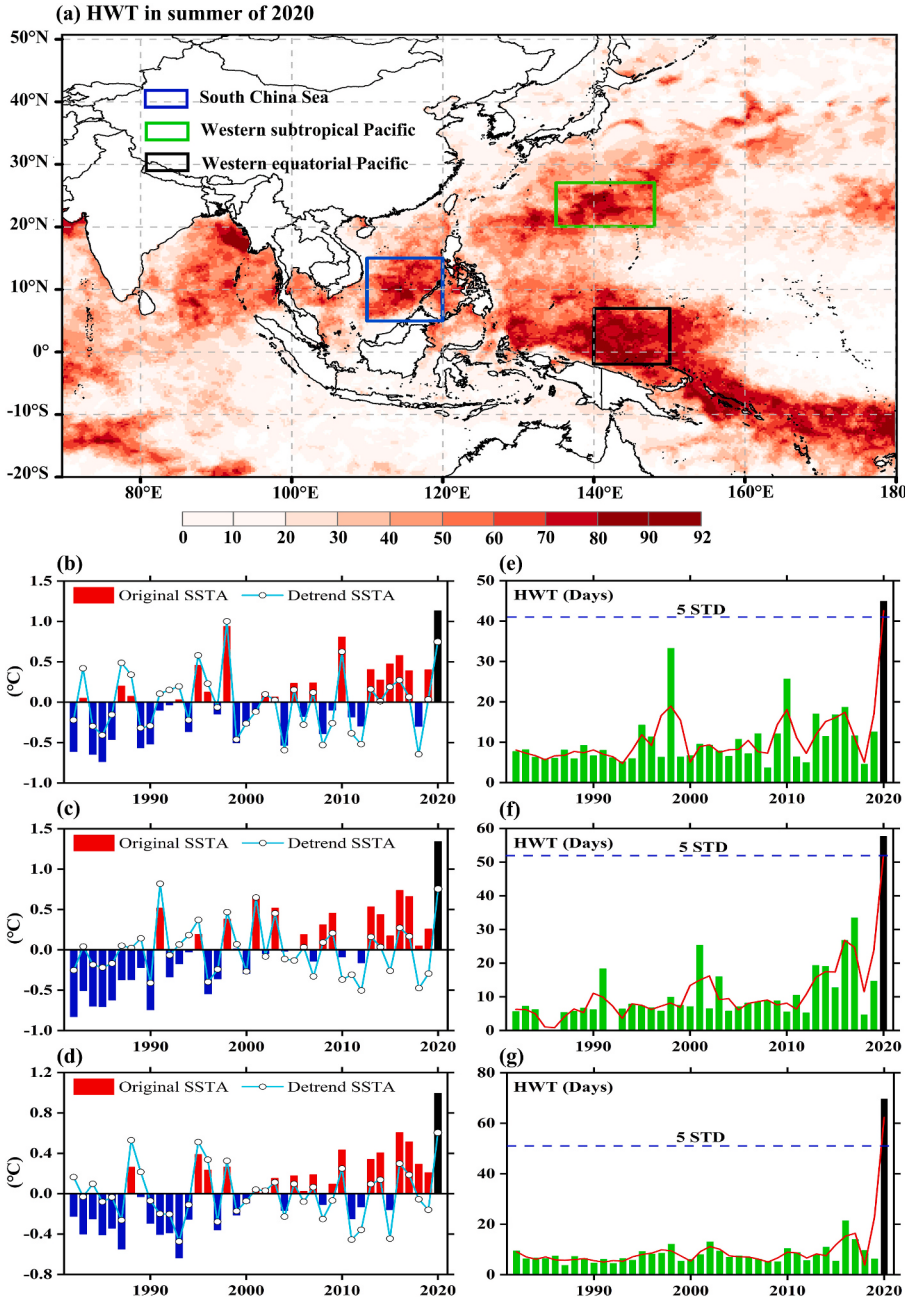


Fig. 1. (a) Spatial distribution of the MHW total days (HWT) in summer 2020 (unit: Days). The blue box denotes the South China Sea (109°E–120°E, 5°N–15°N), the green box denotes the western subtropical Pacific (135°E–148°E, 20°N–27°N), and the black box denotes the western equatorial Pacific (135°E–155°E, 2°S–7°N). Time series of summer regionally aggregated sea surface temperature anomalies (SSTAs) and HWT in (b, e) the South China Sea, (c, f) the western subtropical Pacific, and (d, g) the western equatorial Pacific from 1982 to 2020, respectively. Cyan line with white dots represents the detrended SSTAs, red line represents the 5-year moving average, and blue dashed line represents the 5-standard deviation (STD). The period of the climatological mean is from 1982 to 2020.

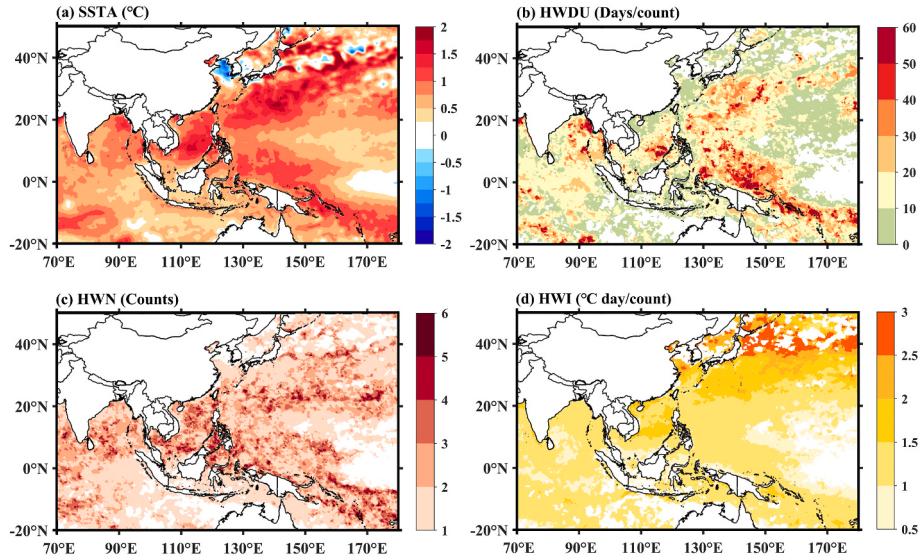


Fig. 2. Spatial distributions of the (a) SST anomaly, (b) average marine heatwave duration (HWDU), (c) number of marine heatwaves (HWN), and (d) average marine heatwave intensity (HWI) in summer (June–July–August) of 2020. The data is from the OISST V2.1.

latitude seas (Fig. 2d). In general, there were record-breaking summer MHWs in the western North Pacific in summer of 2020 and MHWs lasted for the entire summer in parts of the South China Sea and western equatorial Pacific.

3.2. Strengthened western North Pacific subtropical high

MHW occurrence requires favorable large-scale environmental conditions, such as persistent high-pressure systems. Atmospheric blocking

reduces cloud cover, increases insolation, and suppresses surface wind speeds, resulting in hot and dry weather (Holbrook et al., 2020b; Rodrigues et al., 2019). The WNPSH and its corresponding anticyclonic circulation are critical circulation systems that impact the summer East Asian climate (Li et al., 2017; Xie et al., 2016). In June 2020, there was a positive anomaly at the 850-hPa geopotential high, extending westward from 170°E to the South China Sea with strong anticyclonic circulation (Fig. 3a). In July 2020, two positive anomalous centers were formed in the northern Philippine Islands and the eastern Japan Islands. The

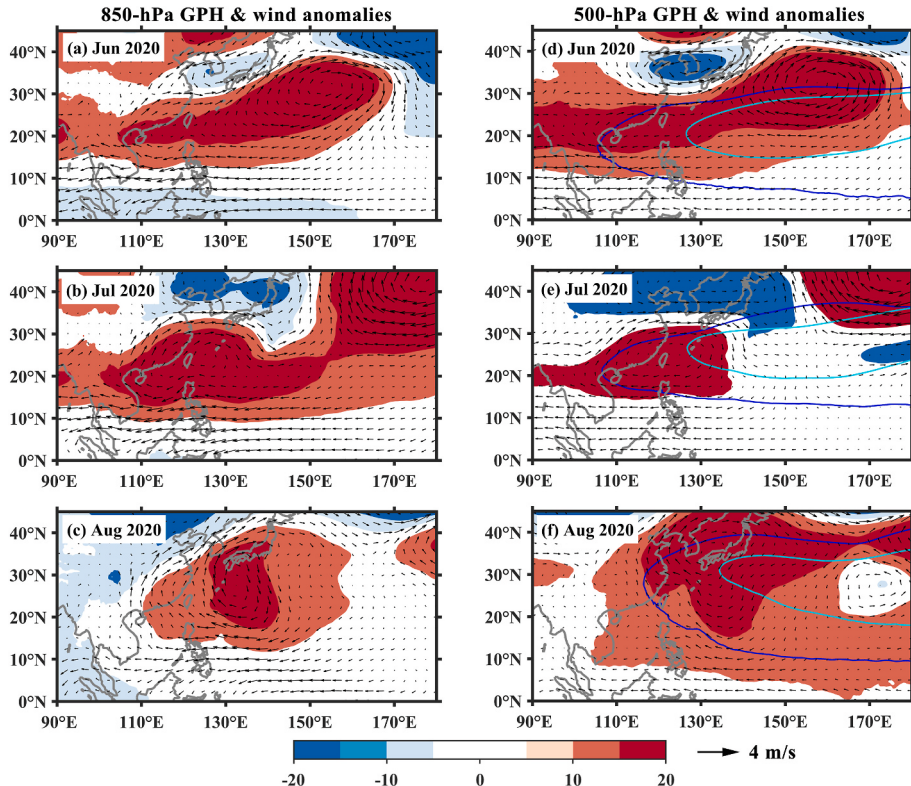


Fig. 3. Spatial patterns of monthly geopotential height (shading, units: gpm) and corresponding wind anomalies (vectors) at 850-hPa (first column) and 500-hPa (second column) in June, July, and August 2020, respectively. Blue lines represent the locations of the monthly average 5880 gpm, and cyan lines represent the locations of the climatological mean of 5880 gpm. The period of the climatological mean is from 1982 to 2020. The data are from the ERA5 reanalysis product.

intensity of the anticyclonic circulation increased, and the coverage area expanded (Fig. 3b). In August 2020, there was only one positive anomaly center in the western subtropical Pacific, and the coverage of the anticyclonic circulation was reduced (Fig. 3c). Like the lower troposphere, the 500-hPa geopotential high also showed a positive anomaly. In June and July 2020, the WNPSH extended westward, and the west ridge point reached 110°E , as far as the northern South China Sea (Fig. 3d–e). In August 2020, the WNPSH moved northward, and its influence on the atmospheric circulation over the South China Sea was weakened (Fig. 3f). The strengthened WNPSH and its westward extension are the most significant large-scale circulation features in summer of 2020.

4. Physical interpretation

4.1. Favorable large-scale conditions over the western North Pacific

Variations in SST over monsoon regions are closely linked to atmospheric forcing (Wang et al., 2005). The most extreme MHW events typically occur in summer when climatological oceanic mixed layers are shallow, and winds are weak (Gupta et al., 2020). Summer MHWs in the South China Sea and western subtropical Pacific are strongly linked to strengthened WNPSH. The high-pressure system enhances short solar radiation, reduces precipitation, suppresses wind speed, increases latent ocean heat loss, and results in hot and dry weather in the western North Pacific (Fig. 4). In summer of 2020, a La Niña-like pattern appeared in the tropical Pacific and developed into a moderate La Niña event in September 2020 (Fig. 5a and Fig. S1a). Additionally, the anticyclonic circulation extends from the western North Pacific to the eastern North Indian Ocean, providing favorable large-scale conditions, such as the easterly wind anomaly, anomalous descending motion, and negative velocity, which jointly trigger SST anomalies in the western North Pacific (Fig. 5a).

The strengthened WNPSH is accompanied by SST warming over the Indian Ocean and the western North Pacific, but SST cooling over the central-eastern equatorial Pacific. Meanwhile, the corresponding outgoing long-wave radiation shows negative anomalies over the tropical Indian Ocean but positive anomalies over the tropical central-western Pacific. SST warming over the tropical Indian Ocean produces anomalous ascending motions and upper-level divergence. The associated upper-level outflows converge toward the western North Pacific, leading to compensating subsidence along with an abnormal anticyclonic circulation (Fig. 5b). The associated surface divergent easterly wind and the high zonal SST gradient over the tropical Pacific strengthen the easterly wind anomaly in the western North Pacific and thus favor the anticyclonic circulation (Chen et al., 2012; Lindzen and Nigam, 1987). Overall, it is reasonable to believe that the anomalous SSTs across the tropical Indian and Pacific Oceans contributed in part to the

strengthening of the WNPSH and the consequent record-breaking MHWs in the western North Pacific during summer 2020.

4.2. Ocean mixed-layer heat budget analysis

In May, the South China Sea and the western subtropical Pacific showed a significant rise in SST anomalies (SSTAs) tendency, with little change in the western equatorial Pacific (Fig. S2). To reflect the previous SST rise, the sum of mixed-layer heat budgets from May to August in the South China Sea and western subtropical Pacific was taken, as well as from June to August in the western equatorial Pacific. The mixed-layer heat budget analysis shows that surface heat flux played a dominant role in the South China Sea and the western subtropical Pacific. In contrast, oceanic heat advection was the main factor regulating the positive SSTA tendencies in the western equatorial Pacific (Fig. 6a, d, g).

After decomposing the oceanic heat advection term, we found that Qu (the zonal advection term) was the leading component and Qv (the meridional advection term) was the positive component in the South China Sea. Qu and Qw (the vertical advection term) were negative components, indicating that the enhanced eastward current and weakened South Vietnam upwelling (Zu et al., 2020) (Fig. 6b). For example, the easterly wind anomalies brought by the anticyclonic circulation weaken the East Asian summer monsoon and cause the summer upwelling to weaken or even disappear off the South Vietnam coast in the South China Sea (Fig. 7). Without the cooling effect of this upwelling, will be a robust basin-wide surface warming, which promotes the occurrence of MHWs (Xie et al., 2003; Yao and Wang, 2021). Notably, atmospheric blocking plays a warming role in the South China Sea by triggering oceanic heat advection. As for the western equatorial Pacific, Qu and Qw were the dominant terms (Fig. 6h). In the middle of 2020, a La Niña-like pattern appeared in the tropical Pacific. The westward current driven by easterly wind anomalies will transport warm water (nearly 6 Sv) to the western Pacific warm pool (Fig. 8). Negative and weak advection in the western subtropical Pacific indicates that oceanic heat advection did not play a significant role (Fig. 6d–e).

In summer of 2020, the decreased latent heat flux and increased solar shortwave radiation anomalies supported the positive net heat flux in the South China Sea and western subtropical Pacific (Fig. 6c, f, and Figs. S3a and c). Increased solar shortwave radiation and suppressed latent and sensible heat fluxes are associated with strengthened WNPSH over the western North Pacific (Fig. 3). However, the increase in latent heat flux counteracts the warming effect of solar shortwave radiation, resulting in a negative role of net heat flux in the western equatorial Pacific (Fig. 6i and Figs. S3e and g). Notably, the residual term in the western equatorial Pacific contributes to a large portion of the warming (Fig. 6g). We infer that the reliability of heat fluxes in the equatorial region is a potential source of this residual term. In addition, the MLD of the western equatorial Pacific changes with the ENSO phase, and the

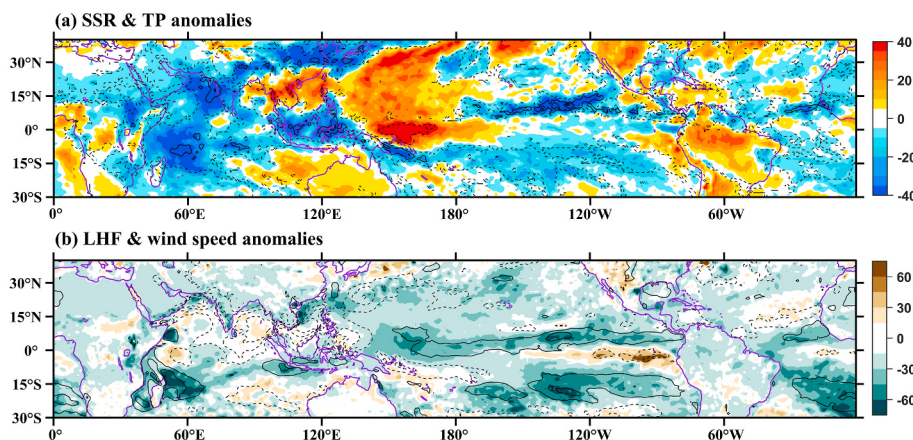


Fig. 4. Large-scale conditions in summer of 2020. (a) Surface net solar radiation (SSR; unit: W/m^2 , downward is positive) and total precipitation (TP; solid lines represent positive values and dotted lines represent negative values) anomalies; (b) surface latent heat flux (LHF; unit: W/m^2 , downward is positive) and 10-m wind speed (solid lines represent positive values and dotted lines represent negative values) anomalies. The period of the climatological mean is from 1982 to 2020. The data are from the ERA5 reanalysis product.

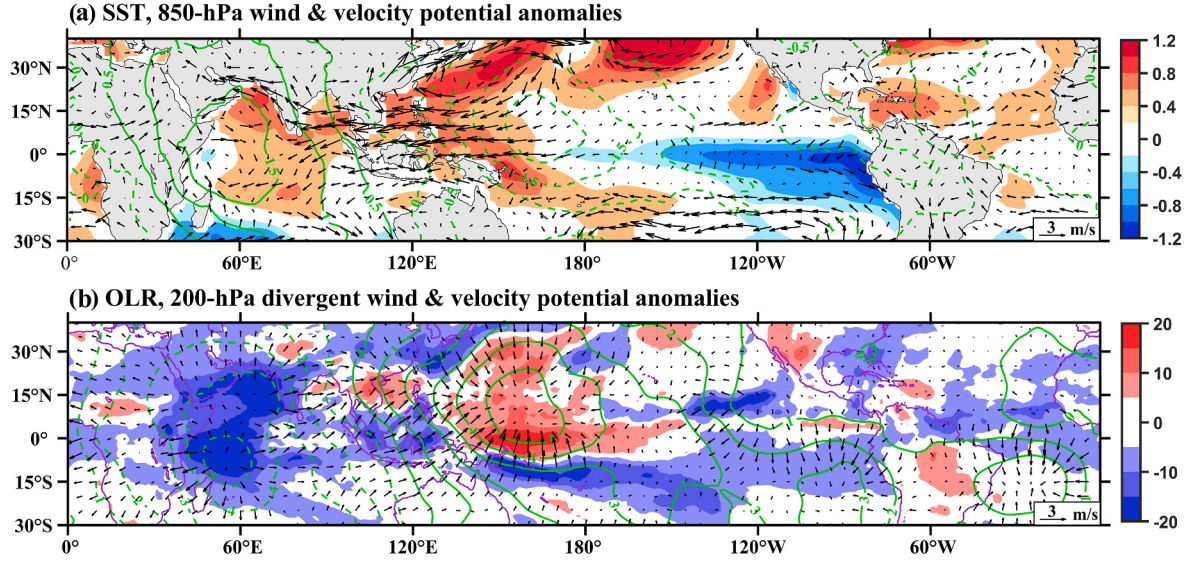


Fig. 5. Large-scale conditions in summer of 2020. (a) anomalous SST (shading, unit: $^{\circ}\text{C}$), 850-hPa wind (vectors), and velocity potential (contour, unit: $10^6 \text{ m}^2 \text{s}^{-1}$); (b) anomalous outgoing long-wave radiation (OLR) (shading, unit: W/m^2), 200-hPa divergent wind (vectors), and velocity potential ($10^6 \text{ m}^2 \text{s}^{-1}$). The period of the climatological mean is from 1982 to 2020. The data are from the ERA5 reanalysis product and ERSST5.

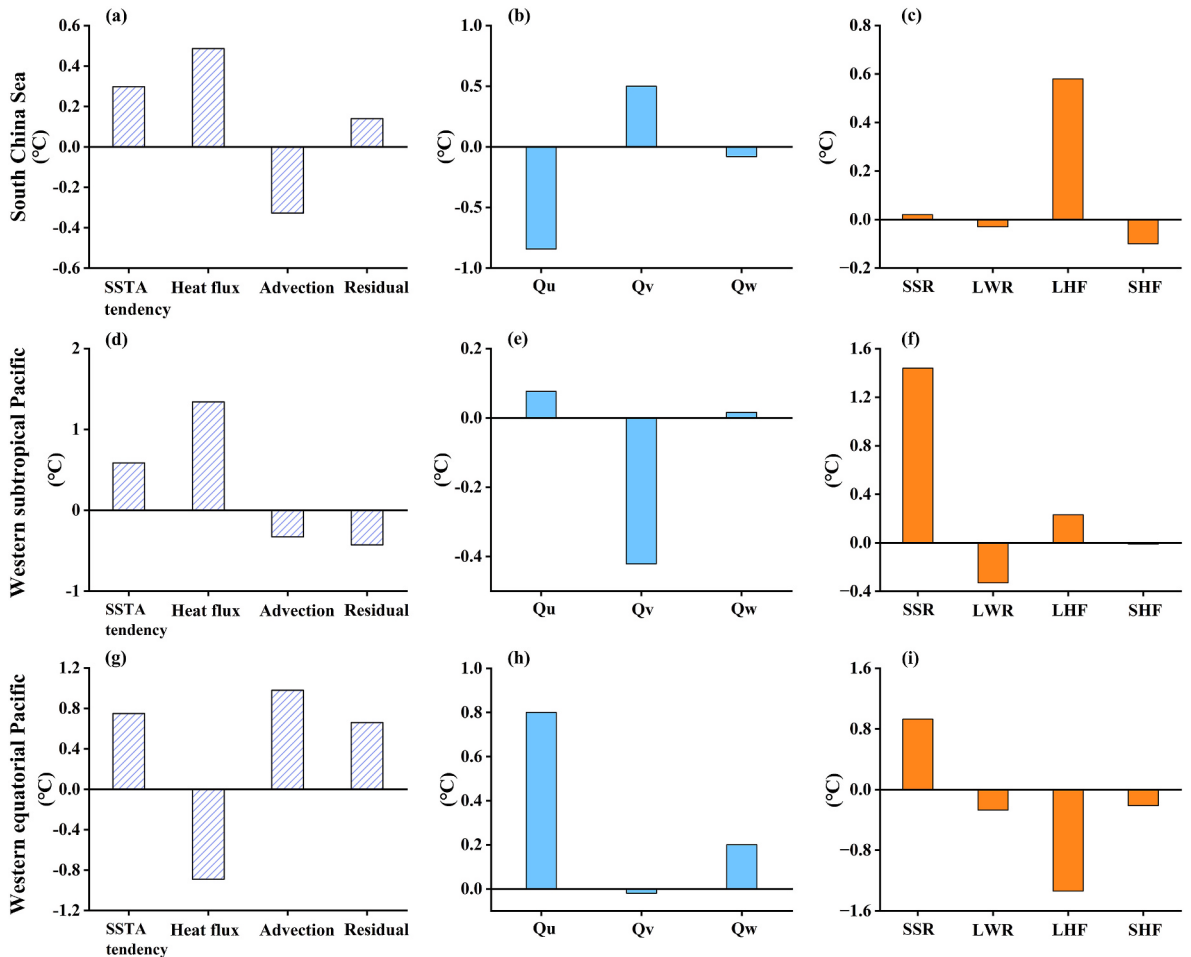


Fig. 6. (a, d, g) The evolution of sum mixed layer heat budget and the decomposition of sum (b, e, h) advection term and (c, f, i) heat flux in (a, b, c) the South China Sea, (d, e, f) the western subtropical Pacific, and (g, h, i) the western equatorial Pacific in summer of 2020 (May-June-July-August for the South China Sea and western subtropical Pacific; June-July-August for the western equatorial Pacific). The heat flux components include net heat flux (NHF), solar shortwave radiation (SSR), longwave radiation (LWR), latent heat flux (LHF), and sensible heat flux (SHF). “Qu” represents the zonal advection term, “Qv” stands for the meridional advection term, and “Qw” is the vertical advection term. The period of the climatological mean is from 1982 to 2020. The heat budget data are from the GODAS ocean reanalysis product, and the heat flux data are from the NCEP-DOE Reanalysis 2 product.

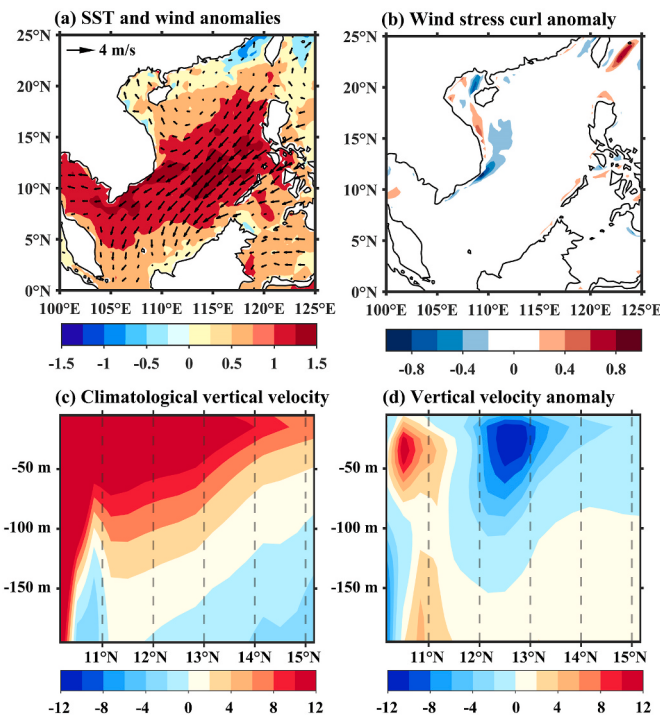


Fig. 7. Summer mean (a) sea surface temperature (SST) (shading, unit: $^{\circ}\text{C}$) and 10-m wind (vectors) anomalies, (b) wind stress curl anomaly (unit: 10^{-6} N/m³) in the South China Sea in 2020, the latitude-depth sections along 110°E of (c) climatological vertical velocity (unit: 10^{-6} m/s), and (d) vertical velocity anomaly (unit: 10^{-6} m/s) in summer of 2020. The period of the climatological mean is from 1982 to 2020. The SST and wind data are from the ERA5 reanalysis product, and the vertical velocity data is from GODAS reanalysis product.

absence of a time-dependent MLD in the heat budget analysis may also increase the residual term (Elzahaby et al., 2022).

In summary, the anomalous WNPSH was responsible for the warm SSTAs in the western North Pacific in summer of 2020, especially in the South China Sea and western subtropical Pacific. Meanwhile, oceanic heat advection plays a dominant role in the western equatorial Pacific. What caused the anomalous WNPSH in summer of 2020?

4.3. Atmospheric model experiments

To test the hypothesized role of trans-basin tropical SST anomalies in the strengthened WNPSH, numerical model experiments were carried out using the ECHAM5 model. The sensitivity experiment generally reproduced the observed atmospheric circulation, such as the anticyclonic circulation and velocity potential anomalies in the western North Pacific. However, there are positive velocity potential anomalies in the tropical Atlantic Ocean, opposite to the observation (Figs. 5c and 9a). The above results indicate that tropical Indian and Pacific Ocean SST anomalies may play a leading role in the strengthened WNPSH.

To further examine the relative contribution of SST anomalies over the tropical oceans, three more sensitivity experiments were carried out by adding SST anomalies from June to August 2020 over the tropical Indian Ocean, Pacific Ocean, and Atlantic Ocean to the corresponding climatological monthly average SST (shading in Fig. 9b–d), respectively. For the tropical Indian Ocean, SST warming can stimulate an anticyclonic circulation by generating local ascending motion and remote descending motion in the western North Pacific (Fig. 9b). The increased SST zonal gradient for the tropical Pacific generates easterly wind anomalies extending from 180° to east of 80°E (Fig. 9c). As for the tropical Atlantic Ocean, SST warming can simulate descending motion over the tropical central Pacific by modulating the Walker circulation. Correspondingly, the surface divergence easterly wind in the central

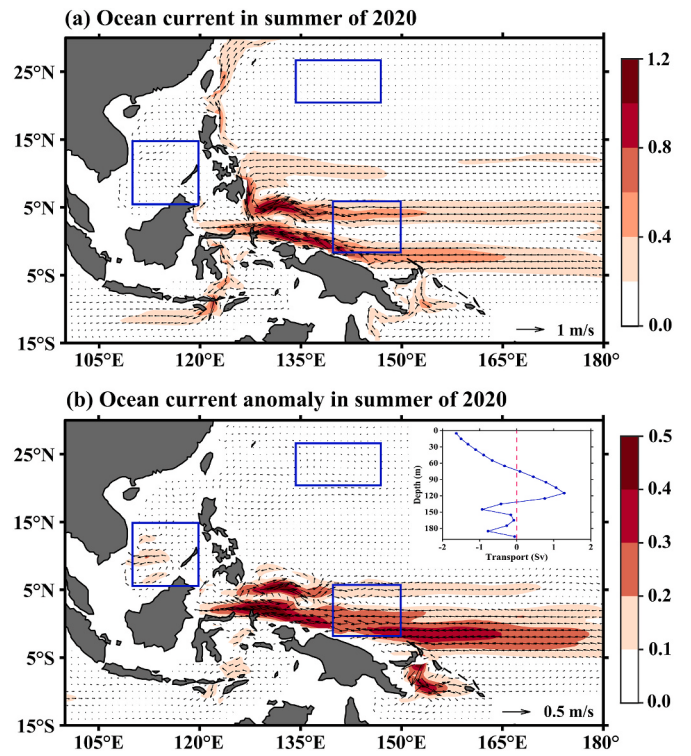


Fig. 8. (a) Ocean current vectors and their magnitude (Shading, units: m/s) averaged at 0–100 m depth in summer of 2020 (June-July-August), and (b) their anomalies. The blue boxes represent the three study areas. The inner graph in (b) shows the vertical variation of zonal warm water transport along 150°E (summed over 5°S–5°N) in summer of 2020. The period of the climatological mean is from 1982 to 2020. The data is from the GODAS reanalysis product.

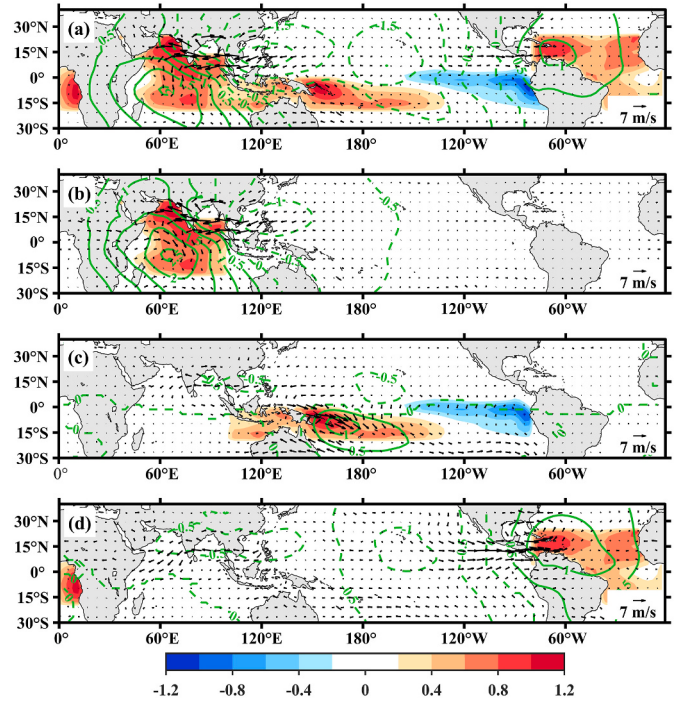


Fig. 9. Prescribed SST (shading, units: $^{\circ}\text{C}$), 850-hPa wind (vectors), and velocity potential (contours, units: $10^6 \text{ m}^2\text{s}^{-1}$) anomalies in response to SST forcings over (a) the tropical oceans, (b) the tropical Indian Ocean, (c) the tropical Pacific Ocean, and (d) the tropical Atlantic Ocean.

Pacific strengthens the anticyclonic circulation over the east part of the western North Pacific as well (Fig. 9d). However, the simulated velocity potential anomalies in the Atlantic Ocean show a positive pattern, opposite to observation (Fig. 5a). Comparing the atmospheric responses to the trans-basin tropical SST anomalies, we find that the tropical Indian Ocean SST warming is dominant in the anomalous anticyclonic circulation. However, the tropical Pacific SSTs also have important contributions. The combination of a La Niña-like pattern in the tropical Pacific and the tropical Indian Ocean can stimulate stronger easterly wind anomalies.

How abnormal is the tropical Indian Ocean SST in summer of 2020 to play a leading role in strengthening the WNPSH? We found that the SST anomaly over the tropical Indian Ocean (10°S – 25°N , 40°E – 100°E) in summer of 2020 was the highest recorded in ERA5 since 1960 and in OISST since 1982, reaching 0.57°C and 0.80°C , respectively. In addition, the SST anomaly in summer of 2020 was the second-highest recorded in ERSST5 since 1960, slightly lower than the previous year (Fig. S4). The record-breaking tropical Indian Ocean SST, coupled with the high tropical Pacific zonal SST gradient, led to the strengthened WNPSH and induced unprecedented MHWs in summer of 2020. Previous studies have suggested that inter-ocean interactions can modulate climate variability through ocean-atmospheric coupling, especially the tropical Indian Ocean warming can trigger an anomalous anticyclone over the western North Pacific during the El Niño decaying summer; besides the ENSO, the tropical Indian Ocean warming and the Indian Ocean dipole also affect the western North Pacific SST (Cai et al., 2019; Wang, 2019; Xie et al., 2009).

5. Implications for the coral bleaching

Coral reefs are the world's most diverse marine ecosystems. They provide billions of dollars in economic value through tourism, coastal protection, and seafood (Costanza et al., 2014; Spalding et al., 2017). However, coral reefs are widely documented as one of the most sensitive marine ecosystems to climate change (Hoegh-Guldberg et al., 2007). Under extreme thermal stress, coral reefs expel their symbiotic algae and color, often leads to widespread mortality. This phenomenon is known as coral bleaching (Fordyce et al., 2019). For over two decades, the DHWs product of the NOAA Coral Reef Watch has been the standard metric for measuring and predicting accumulated thermal stress in coral reef environments (Liu et al., 2014). Predictions of mild and severe coral bleaching are standard at DHWs of 4°C -weeks and 8°C -weeks, respectively.

In summer 2020, DHWs exceeded 4°C -weeks in most South China Sea, the western subtropical Pacific, and a small part of the western equatorial Pacific. Notably, the DHWs have reached mortality-level thermal stress in the northeastern South China Sea (Fig. 10a). Previous studies have reported coral bleaching in the Beibu Gulf (Chen et al., 2022; Feng et al., 2022; Lyu et al., 2022; Mo et al., 2022), the Nansha Islands (Yao and Wang, 2021), western Luzon in the Philippines (Licuanan and Mordeno, 2021), and Northeast Peninsular Malaysia (Szereday and Amri, 2021) in summer of 2020.

Although the DHW index has shown great power in monitoring coral bleaching, it does not always detect intense, acute events that can cause significant coral bleaching (Fordyce et al., 2019). In most of the western North Pacific, the total MHW days was more than a month in summer of 2020, and some regions experienced almost the entire summer MHWs. Reported coral bleaching in the South China Sea has a better spatial correspondence with a high value of total MHW days in summer 2020 compared with DHWs (Fig. 10b). Furthermore, this phenomenon was also present in some previous years of mass coral bleaching (Figs. S5 and 6). Therefore, examining heat stress in coral reef environments using the MHW approach may be a powerful tool for detecting and measuring coral bleaching (Fordyce et al., 2019; Genevier et al., 2019). In addition, it is essential to combine MHWs with DHWs to improve our ability to predict coral bleaching events.

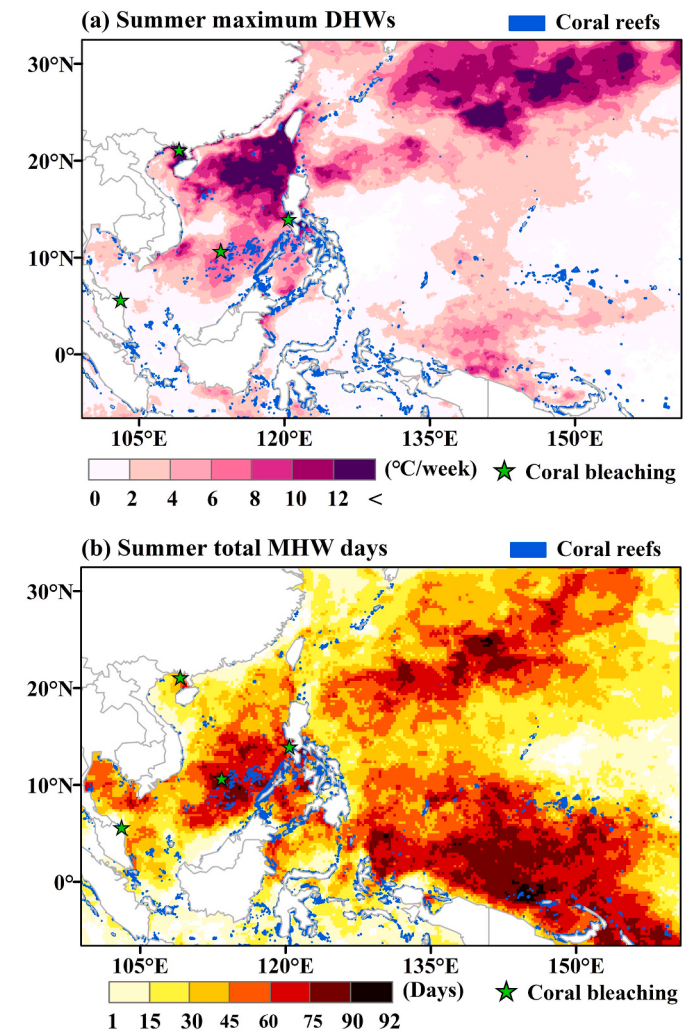


Fig. 10. Spatial patterns of (a) the summer mean degree heating weeks and (b) summer total MHW days in the western North Pacific in 2020. The blue shading displays the location of the coral reefs. The stars represent locations with reports of coral bleaching in summer of 2020.

6. Conclusion and discussion

Record-breaking MHWs occurred in the western North Pacific in summer of 2020. This unprecedented phenomenon is consistent with favorable large-scale conditions strongly linked to the strengthened WNPSH and a La Niña-like pattern in the Pacific Ocean. Inter-ocean SST anomalies in the tropical oceans are the main causes, with the Indian Ocean playing a leading role. Meanwhile, the oceanic heat advection in the western equatorial Pacific and South China Sea also contribute to seawater warming (Fig. 11). The tropical Indian Ocean SST warming generates anomalous ascending motions and upper-level divergence, with the associated upper-level outflows converging toward the western North Pacific, which results in compensation for sinking air associated with an anomalous high in the western North Pacific. The related surface divergent easterly wind and the zonal SST gradient increase in the tropical Pacific Ocean strengthened the anomalous easterly trade winds in the western North Pacific, which is conducive to the anomalous anticyclonic circulation. Furthermore, numerical model experiments found that the trans-basin tropical SST can produce favorable large-scale conditions, with tropical Indian Ocean SST warming playing a leading role in anomalous anticyclonic circulation.

The WNPSH is an important atmospheric circulation system that conveys El Niño events' impacts on the East Asian summer climate. The

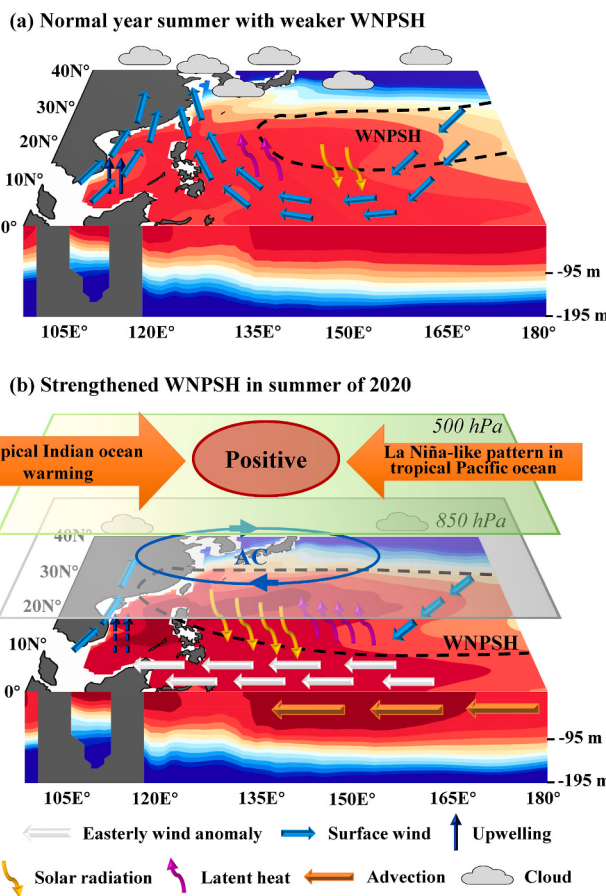


Fig. 11. Schematic of physical mechanism associated with MHWs in the western North Pacific. (a) In normal summer, weaker western North Pacific subtropical high (WNPSH) and strong East Asian summer monsoon; (b) severe summer MHWs in western Northwest Pacific in summer of 2020. The strengthened WNPSH and its corresponding anticyclonic circulation (AC), and the easterly wind anomalies transport warm seawater from the equatorial eastern Pacific to the western equatorial Pacific.

central Pacific cold SST anomaly may induce anticyclonic circulation during rapid El Niño decay/La Niña development or if La Niña persists through the summer (Chen et al., 2016; Li et al., 2017). However, in 2019/20 winter, the Niño3.4 index was at only 0.5 °C with a weak intensity El Niño event, which is insufficient to induce a robust anomalous WNPSH. The model's simulation results indicate that the strengthened WNPSH is mainly due to the tropical Indian Ocean SST anomaly. So, the question naturally follows what caused the Indian Ocean warming? The record-strong downwelling Rossby waves excited by the 2019 super Indian Ocean Dipole may have contributed to the tropical Indian Ocean SST warming in summer of 2020 (Takaya et al., 2020; Zhou et al., 2021). Moreover, anthropogenic greenhouse gas emissions also increased the probability of the highest SSTs observed in the western North Pacific (Hayashi et al., 2021).

The Indian Ocean is projected to warm more in response to anthropogenic activities. The tropical Indian Ocean SST warming may be relatively higher than that of the tropical Pacific Ocean under global warming (Xie et al., 2010, 2016). Furthermore, the WNPSH will intensify robustly in the future (Chen et al., 2020; He et al., 2022). Therefore, combining the Indian Ocean and WNPSH may make severe MHWs more frequent in the western North Pacific under a global warming background. Meanwhile, climate change impacts on coral reefs are expected to include extensive coral bleaching events. It is critical to consider MHWs as a powerful tool in detecting acute, intense thermal stress events in the coral bleaching pre-warning system.

Authorship contribution statement

Yulong Yao: Conceptualization, Methodology, Visualization, Writing – original draft. Chunzai Wang: Supervision, Writing – review & editing. Chao Wang: Methodology, Software, Writing – review & editing.

Declaration of competing interest

The authors declare that they have no known competing financial interests or personal relationships that could have appeared to influence the work reported in this paper.

Data availability

Data will be made available on request.

Acknowledgements

This research is supported by the National Natural Science Foundation of China (42192562), the National Key R&D Program of China (2019YFA0606701), the National Natural Science Foundation of China (42192564 & 42106202), the Strategic Priority Research Program of the Chinese Academy of Sciences (XDB42000000 & XDA20060502), the Innovation Academy of South China Sea Ecology and Environmental Engineering, the Chinese Academy of Sciences (ISEE2021ZD01), the Independent Research Project Program of State Key Laboratory of Tropical Oceanography (LTOZZ2201), and development fund of South China Sea Institute of Oceanology of the Chinese Academy of Sciences (SCSIO202208). The numerical computation is supported by the High Performance Computing Division in the South China Sea Institute of Oceanology.

The OISST v2.1 is publicly available at <https://www.ncei.noaa.gov/thredds/catalog/OisstBase/NetCDF/V2.1/AVHRR/catalog.html>; ERSST v5 is at <https://psl.noaa.gov/data/gridded/data.noaa.ersst.v5.html>; ERA5 is at <https://www.ecmwf.int/en/forecasts/datasets/reanalysis-datasets/era5>; GODAS data is at <https://www.psl.noaa.gov/data/gridded/data.godas.html>; NCEP/DOE 2 Reanalysis data is available at <https://psl.noaa.gov/data/gridded/data.ncep.reanalysis2.gaussian.html>; Degree heating weeks data is download from https://www.star.nesdis.noaa.gov/pub/sod/mecb/crw/data/5km/v3.1_op/nc/v1.0/daily/dhw/. The simulation data are available at <https://zenodo.org/record/6529780#.Ynh22YxBxGM> (DOI: 10.5281/zenodo.6529780).

Appendix A. Supplementary data

Supplementary data to this article can be found online at <https://doi.org/10.1016/j.dsr2.2023.105288>.

References

- Cai, W., Wu, L., Lengaigne, M., Li, T., McGregor, S., Kug, J.-S., Yu, J.-Y., Stuecker, M.F., Santoso, A., Li, X., 2019. Pantropical climate interactions. *Science* 363. <https://doi.org/10.1126/science.aav4236>.
- Chen, M., Li, T., Shen, X., Wu, B., 2016. Relative roles of dynamic and thermodynamic processes in causing evolution asymmetry between El Niño and La Niña. *J. Clim.* 29, 2201–2220. <https://doi.org/10.1175/JCLI-D-15-0547.1>.
- Chen, W., Park, J.K., Dong, B., Lu, R., Jung, W.S., 2012. The relationship between El Niño and the western North Pacific summer climate in a coupled GCM: role of the transition of El Niño decaying phases. *J. Geophys. Res. Atmos.* 117, D12111 <https://doi.org/10.1029/2011JD017385>.
- Chen, X., Zhou, T., Wu, P., Guo, Z., Wang, M., 2020. Emergent constraints on future projections of the western North Pacific subtropical high. *Nat. Commun.* 11, 2802. <https://doi.org/10.1038/s41467-020-16631-9>.
- Chen, Y., Zhai, F., Li, P., Gu, Y., Wu, K., 2022. Extreme 2020 summer SSTs in the northern South China Sea: implications for the Beibu Gulf coral bleaching. *J. Clim.* 35, 4177–4190. <https://doi.org/10.1175/JCLI-D-21-0649.1>.
- Cheng, L., Abraham, J., Hausfather, Z., Trenberth, K.E., 2019. How fast are the oceans warming? *Science* 363, 128–129. <https://doi.org/10.1126/science.aav7619>.

- Cheng, L., Abraham, J., Trenberth, K.E., Fasullo, J., Boyer, T., Locarnini, R., Zhang, B., Yu, F., Wan, L., Chen, X., 2021. Upper ocean temperatures hit record high in 2020. *Adv. Atmos. Sci.* 38, 523–530. <https://doi.org/10.1007/s00376-021-0447-x>.
- Cheng, L., Trenberth, K.E., Fasullo, J., Boyer, T., Abraham, J., Zhu, J., 2017. Improved estimates of ocean heat content from 1960 to 2015. *Sci. Adv.* 3, e1601545 <https://doi.org/10.1126/sciadv.1601545>.
- Costanza, R., De Groot, R., Sutton, P., Van der Ploeg, S., Anderson, S.J., Kubiszewski, I., Farber, S., Turner, R.K., 2014. Changes in the global value of ecosystem services. *Global Environ. Change* 26, 152–158. <https://doi.org/10.1016/j.gloenvcha.2014.04.002>.
- Elzahaby, Y., Schaeffer, A., Roughan, M., Delaix, S., 2022. Why the mixed layer depth matters when diagnosing marine heatwave drivers using a heat budget approach. *Front. Clim.* 4, 838017 <https://doi.org/10.3389/fclim.2022.838017>.
- Fan, H., Huang, B., Yang, S., Li, Z., Deng, K., 2019. Seasonally-dependent impact of easterly wind bursts on the development of El Niño events. *Clim. Dynam.* 53, 1527–1546. <https://doi.org/10.1007/s00382-019-04688-2>.
- Feng, Y., Bethel, B.J., Dong, C., Zhao, H., Yao, Y., Yu, Y., 2022. Marine heatwave events near Weizhou Island, Beibu Gulf in 2020 and their possible relations to coral bleaching. *Sci. Total Environ.* 823, 153414 <https://doi.org/10.1016/j.scitotenv.2022.153414>.
- Fordyce, A.J., Ainsworth, T.D., Heron, S.F., Leggat, W., 2019. Marine heatwave hotspots in coral reef environments: physical drivers, ecophysiological outcomes, and impact upon structural complexity. *Front. Mar. Sci.* 6, 498. <https://doi.org/10.3389/fmars.2019.00498>.
- Gao, G., Marin, M., Feng, M., Yin, B., Yang, D., Feng, X., Ding, Y., Song, D., 2020. Drivers of marine heatwaves in the East China Sea and the South Yellow Sea in three consecutive summers during 2016–2018. *J. Geophys. Res. Oceans* 125, e2020JC016518. <https://doi.org/10.1029/2020JC016518>.
- Genevier, L.G., Jamil, T., Raitsos, D.E., Krokos, G., Hoteit, I., 2019. Marine heatwaves reveal coral reef zones susceptible to bleaching in the Red Sea. *Global Change Biol.* 25, 2338–2351. <https://doi.org/10.1111/gcb.14652>.
- Gupta, A.S., Thomsen, M., Benthuysen, J.A., Hobday, A.J., Oliver, E., Alexander, L.V., Burrows, M.T., Donat, M.G., Feng, M., Holbrook, N.J., 2020. Drivers and impacts of the most extreme marine heatwaves events. *Sci. Rep.* 10, 19359 <https://doi.org/10.1038/s41598-020-75445-3>.
- Hayashi, M., Shioigama, H., Emori, S., Ogura, T., Hirota, N., 2021. The Northwestern Pacific warming record in August 2020 occurred under anthropogenic forcing. *Geophys. Res. Lett.* 48, e2020GL090956. <https://doi.org/10.1029/2020GL090956>.
- He, C., Cui, Z., Wang, C., 2022. Response of western North Pacific anomalous anticyclones in the summer of decaying El Niño to global warming: diverse projections based on CMIP6 and CMIP5 models. *J. Clim.* 35, 359–372. <https://doi.org/10.1175/JCLI-D-21-0352.1>.
- Hobday, A.J., Alexander, L.V., Perkins, S.E., Smale, D.A., Straub, S.C., Oliver, E.C., Benthuysen, J.A., Burrows, M.T., Donat, M.G., Feng, M., 2016. A hierarchical approach to defining marine heatwaves. *Prog. Oceanogr.* 141, 227–238. <https://doi.org/10.1016/j.pocean.2015.12.014>.
- Hoegh-Guldberg, O., Mumby, P.J., Hooten, A.J., Steneck, R.S., Greenfield, P., Gomez, E., Harvell, C.D., Sale, P.F., Edwards, A.J., Caldeira, K., 2007. Coral reefs under rapid climate change and ocean acidification. *Science* 318, 1737–1742. <https://doi.org/10.1126/science.1152509>.
- Holbrook, N.J., Claar, D.C., Hobday, A.J., McInnes, K.L., Oliver, E.C., Gupta, A.S., Widlansky, M.J., Zhang, X., 2020a. ENSO-Driven Ocean Extremes and Their Ecosystem Impacts. El Niño Southern Oscillation in a Changing Climate, pp. 409–428. <https://doi.org/10.1002/9781119548164.ch18>.
- Holbrook, N.J., Gupta, A.S., Oliver, E.C., Hobday, A.J., Benthuysen, J.A., Scannell, H.A., Smale, D.A., Wernberg, T., 2020b. Keeping pace with marine heatwaves. *Nat. Rev. Earth Environ.* 1, 482–493. <https://doi.org/10.1038/s43017-020-0068-4>.
- Holbrook, N.J., Scannell, H.A., Gupta, A.S., Benthuysen, J.A., Feng, M., Oliver, E.C., Alexander, L.V., Burrows, M.T., Donat, M.G., Hobday, A.J., 2019. A global assessment of marine heatwaves and their drivers. *Nat. Commun.* 10, 2624. <https://doi.org/10.1038/s41467-019-10206-z>.
- Huang, B., Liu, C., Banzon, V., Freeman, E., Graham, G., Hankins, B., Smith, T., Zhang, H.-M., 2021. Improvements of the daily optimum interpolation sea surface temperature (DOISST) version 2.1. *J. Clim.* 34, 1–47. <https://doi.org/10.1175/JCLI-D-20-0166.1>.
- Huang, B., Thorne, P.W., Banzon, V.F., Boyer, T., Chepurin, G., Lawrimore, J.H., Menne, M.J., Smith, T.M., Vose, R.S., Zhang, H.-M., 2017. Extended reconstructed sea surface temperature, version 5 (ERSSTv5): upgrades, validations, and intercomparisons. *J. Clim.* 30, 8179–8205. <https://doi.org/10.1175/JCLI-D-16-0836.1>.
- Huang, B., Xue, Y., Zhang, D., Kumar, A., McPhaden, M.J., 2010. The NCEP GODAS ocean analysis of the tropical Pacific mixed layer heat budget on seasonal to interannual time scales. *J. Clim.* 23, 4901–4925. <https://doi.org/10.1175/2010JCLI3373.1>.
- Kanamitsu, M., Ebisuzaki, W., Woollen, J., Yang, S.-K., Hnilo, J., Fiorino, M., Potter, G., 2002. Ncep-doe amip-ii reanalysis (R-2). *Bull. Am. Meteorol. Soc.* 83, 1631–1644. <https://doi.org/10.1175/BAMS-83-11-1631>.
- Li, T., Wang, B., Wu, B., Zhou, T., Chang, C.-P., Zhang, R., 2017. Theories on formation of an anomalous anticyclone in western North Pacific during El Niño: a review. *J. Meteorol. Res.* 31, 987–1006. <https://doi.org/10.1007/s13351-017-7147-6>.
- Licuanan, W.Y., Mordeno, P.Z.B., 2021. Citizen science reveals the prevalence of the 2020 mass coral bleaching in one town. *Philipp. J. Sci.* 150, 945–949. https://phijournals.dost.gov.ph/images/pdf/pjs_pdf/vol150no3/citizen_science_reveals_th_prevalence_of_mass_coral_bleaching.pdf.
- Lindzen, R.S., Nigam, S., 1987. On the role of sea surface temperature gradients in forcing low-level winds and convergence in the tropics. *J. Atmos. Sci.* 44, 2418–2436. [https://doi.org/10.1175/1520-0469\(1987\)044%3C2418:OTROSS%3E2.0.CO;2](https://doi.org/10.1175/1520-0469(1987)044%3C2418:OTROSS%3E2.0.CO;2).
- Liu, G., Heron, S.F., Eakin, C.M., Muller-Karger, F.E., Vega-Rodriguez, M., Guild, L.S., De La Cour, J.L., Geiger, E.F., Skirving, W.J., Burgess, T.F., 2014. Reef-scale thermal stress monitoring of coral ecosystems: new 5-km global products from NOAA Coral Reef Watch. *Rem. Sens.* 6, 11579–11606. <https://doi.org/10.3390/rs61111579>.
- Liu, K., Xu, K., Zhu, C., Liu, B., 2022. Diversity of marine heatwaves in the South China Sea regulated by ENSO phase. *J. Clim.* 35, 877–893. <https://doi.org/10.1175/JCLI-D-21-0309.1>.
- Liu, Y., Weisberg, R.H., Law, J., Huang, B., 2018. Evaluation of satellite-derived SST products in identifying the rapid temperature drop on the West Florida Shelf associated with hurricane Irma. *Mar. Technol. Soc. J.* 52 (3), 43–50. <https://doi.org/10.4031/MTSJ.52.3.7>.
- Lyu, Y., Zhou, Z., Zhang, Y., Chen, Z., Deng, W., Shi, R., 2022. The mass coral bleaching event of inshore corals form South China Sea witnessed in 2020: insight into the causes, process and consequence. *Coral Reefs.* <https://doi.org/10.1007/s00338-022-02284-1>.
- Mo, S., Chen, T., Chen, Z., Zhang, W., Li, S., 2022. Marine heatwaves impair the thermal refugia potential of marginal reefs in the northern South China Sea. *Sci. Total Environ.* 825, 154100. <https://doi.org/10.1016/j.scitotenv.2022.154100>.
- Oliver, E.C., Benthuysen, J.A., Darmaraki, S., Donat, M.G., Hobday, A.J., Holbrook, N.J., Schlegel, R.W., Gupta, A.S., 2020. Marine heatwaves. *Ann. Rev. Mar. Sci.* 13, 313–342. <https://doi.org/10.1146/annurev-marine-032720-095144>.
- Oliver, E.C., Donat, M.G., Burrows, M.T., Moore, P.J., Smale, D.A., Alexander, L.V., Benthuysen, J.A., Feng, M., Gupta, A.S., Hobday, A.J., 2018. Longer and more frequent marine heatwaves over the past century. *Nat. Commun.* 9, 1324. <https://doi.org/10.1038/s41467-018-03732-9>.
- Rodrigues, R.R., Taschetto, A.S., Gupta, A.S., Foltz, G.R., 2019. Common cause for severe droughts in South America and marine heatwaves in the South Atlantic. *Nat. Geosci.* 12, 620–626. <https://doi.org/10.1038/s41561-019-0393-8>.
- Roeckner, E., Bäuml, G., Bonaventura, L., Brokopf, R., Esch, M., Giorgi, M., Hagemann, S., Kirchner, I., Kornblueh, L., Manzini, E., 2003. The Atmospheric General Circulation Model ECHAM 5. PART I: Model Description, vol. 349. Report/Max-Planck-Institut für Meteorologie. <http://hdl.handle.net/11858/00-001M-0000-0012-0144-5>.
- Smale, D.A., Wernberg, T., Oliver, E.C., Thomsen, M., Harvey, B.P., Straub, S.C., Burrows, M.T., Alexander, L.V., Benthuysen, J.A., Donat, M.G., 2019. Marine heatwaves threaten global biodiversity and the provision of ecosystem services. *Nat. Clim. Change* 9, 306–312. <https://doi.org/10.1038/s41558-019-0412-1>.
- Souter, D., Planes, S., Wicquart, J., Logan, M., Obura, D., Staub, F., 2022. Status of Coral Reefs of the World: 2020. Global Coral Reef Monitoring Network. <https://gcrn.net/wp-content/uploads/2021/10/Executive-Summary-with-Forewords.pdf>.
- Spalding, M., Burke, L., Wood, S.A., Ashpole, J., Hutchison, J., Zu Ermgassen, P., 2017. Mapping the global value and distribution of coral reef tourism. *Mar. Pol.* 82, 104–113. <https://doi.org/10.1016/j.marpol.2017.05.014>.
- Szereday, S., Amri, A.Y., 2021. Successive Bleaching Events (2019–2020) in Northeast Peninsular Malaysia Revealed Selective Thermal Acclimatization and Susceptibility of Hard Corals at Biophysical Reef Scale. *bioRxiv*. <https://doi.org/10.1101/2021.11.16.468775>.
- Takaya, Y., Ishikawa, I., Kobayashi, C., Endo, H., Ose, T., 2020. Enhanced Meiyu-Baiu rainfall in early summer 2020: aftermath of the 2019 super IOD event. *Geophys. Res. Lett.* 47, e2020GL090671. <https://doi.org/10.1029/2020GL090671>.
- Tan, H., Cai, R., 2018. What caused the record-breaking warming in East China Seas during August 2016? *Atmos. Sci. Lett.* 19, e853. <https://doi.org/10.1002/asl.853>.
- Wang, B., Ding, Q., Fu, X., Kang, I.S., Jin, K., Shukla, J., Doblas-Reyes, F., 2005. Fundamental challenge in simulation and prediction of summer monsoon rainfall. *Geophys. Res. Lett.* 32, L15711. <https://doi.org/10.1029/2005GL022734>.
- Wang, C., 2019. Three-ocean interactions and climate variability: a review and perspective. *Clim. Dynam.* 53, 5119–5136. <https://doi.org/10.1007/s00382-019-04930-x>.
- Wang, C., Wu, K., Wu, L., Zhao, H., Cao, J., 2021. What caused the unprecedented absence of western North Pacific tropical cyclones in July 2020? *Geophys. Res. Lett.* 48, e2020GL092282. <https://doi.org/10.1029/2020GL092282>.
- Wu, B., Zhou, T., Li, T., 2017. Atmospheric dynamic and thermodynamic processes driving the western North Pacific anomalous anticyclone during El Niño. Part I: maintenance mechanisms. *J. Clim.* 30, 9621–9635. <https://doi.org/10.1175/JCLI-D-16-0489.1>.
- Xie, S.-P., Deser, C., Vecchi, G.A., Ma, J., Teng, H., Wittenberg, A.T., 2010. Global warming pattern formation: sea surface temperature and rainfall. *J. Clim.* 23, 966–986. <https://doi.org/10.1175/2009JCLI3291.1>.
- Xie, S.-P., Hu, K., Hafner, J., Tokinaga, H., Du, Y., Huang, G., Sampe, T., 2009. Indian Ocean capacitor effect on Indo-western Pacific climate during the summer following El Niño. *J. Clim.* 22, 730–747. <https://doi.org/10.1175/2008JCLI2544.1>.
- Xie, S.-P., Kosaka, Y., Du, Y., Hu, K., Chowdry, J.S., Huang, G., 2016. Indo-western Pacific Ocean capacitor and coherent climate anomalies in post-ENSO summer: a review. *Adv. Atmos. Sci.* 33, 411–432. <https://doi.org/10.1007/s00376-015-5192-6>.
- Xie, S.-P., Xie, Q., Wang, D., Liu, W.T., 2003. Summer upwelling in the South China Sea and its role in regional climate variations. *J. Geophys. Res. Oceans* 108, 3261. <https://doi.org/10.1029/2003JC001867>.
- Yao, Y., Wang, C., 2021. Variations in summer marine heatwaves in the South China sea. *J. Geophys. Res. Oceans* 126, e2021JC017792. <https://doi.org/10.1029/2021JC017792>.
- Yao, Y., Wang, J., Yin, J., Zou, X., 2020. Marine heatwaves in China's marginal seas and adjacent Offshore waters: past, present, and future. *J. Geophys. Res. Oceans* 125, e2019JC015801. <https://doi.org/10.1029/2019JC015801>.

- Zhou, Z.-Q., Xie, S.-P., Zhang, R., 2021. Historic Yangtze flooding of 2020 tied to extreme Indian Ocean conditions. Proc. Natl. Acad. Sci. U.S.A. 118, e2022255118 <https://doi.org/10.1073/pnas.2022255118>.
- Zhu, J., Kumar, A., 2018. Influence of surface nudging on climatological mean and ENSO feedbacks in a coupled model. Clim. Dynam. 50, 571–586. <https://doi.org/10.1007/s00382-017-3627-8>.
- Zu, T., Wang, D., Wang, Q., Li, M., Wei, J., Geng, B., He, Y., Chen, J., 2020. A revisit of the interannual variation of the South China Sea upper layer circulation in summer: correlation between the eastward jet and northward branch. Clim. Dynam. 54, 457–471. <https://doi.org/10.1007/s00382-019-05007-5>.